The Astrophysical Journal, 889:45 (11pp), 2020 January 20 https://doi.org/10.3847/1538-4357/ab5b00

Eating Planets for Lunch and Dinner: Signatures of Planet Consumption by Evolving Stars

Alexander P. Stephan[1,2], Smadar Naoz[1,2], B. Scott Gaudi[3], and Jesus M. Salas[1,2]
[1] Department of Physics and Astronomy, University of California, Los Angeles, Los Angeles, CA 90095, USA; alexpstephan@astro.ucla.edu
[2] Mani L. Bhaumik Institute for Theoretical Physics, University of California, Los Angeles, Los Angeles, CA 90095, USA
[3] Department of Astronomy, The Ohio State University, Columbus, OH 43210, USA
Received 2019 September 11; revised 2019 November 21; accepted 2019 November 21; published 2020 January 23

Abstract

Exoplanets have been observed around stars at all stages of stellar evolution, in many cases orbiting in configurations that will eventually lead to the planets being engulfed or consumed by their host stars, such as hot Jupiters or ultrashort period planets. Furthermore, objects such as polluted white dwarfs provide strong evidence that the consumption of planets by stars is a common phenomenon. This consumption causes several significant changes in the stellar properties, such as changes to the stellar spin, luminosity, chemical composition, or mass-loss processes. Here, we explore this wide variety of effects for a comprehensive range of stellar and planetary masses and stages of stellar evolution, from the main sequence over red giants to white dwarfs. We determine that planet consumption can cause transient luminosity features that last on the order of centuries to millennia, and that the post-consumption stellar spins can often reach breakup speeds. Furthermore, stellar mass loss can be caused by this spin-up, as well as through surface grazing interactions, leading to to the formation of unusual planetary nebula shapes or collimated stellar gas ejections. Our results highlight several observable stellar features by which the presence or previous existence of a planet around a given star can be deduced. This will provide future observational campaigns with the tools to better constrain exoplanet demographics, as well as planetary formation and evolution histories.

Unified Astronomy Thesaurus concepts: Stellar evolution (1599); Stellar rotation (1629); Tidal interaction (1699)

1. Introduction

Exoplanets have been observed around a variety of host stars, at all stages of stellar evolution, including main-sequence (MS), subgiant, and red giant branch stars (e.g., Charpinet et al. 2011; Johnson et al. 2011; Gettel et al. 2012; Howard et al. 2012; Barnes et al. 2013; Nowak et al. 2013; Reffert et al. 2015; Niedzielski et al. 2015, 2016). Additionally, white dwarf pollution signatures may indicate the presence of planetary systems in a large fraction of white dwarf systems (about 25% to 50%, e.g., Jura et al. 2009; Klein et al. 2010, 2011; Zuckerman et al. 2010; Melis et al. 2011). Planets that stray too close to their host star may get disrupted and finally consumed by the star (e.g., WASP-12b Patra et al. 2017), leading, for example, to the observed white dwarf pollution (e.g., Vanderburg et al. 2015).

Dynamical processes play an important role in planetary system formation and evolution, in particular planet consumption. Interactions between planets may result in orbital instability, possibly plunging planets into the star (e.g., Rasio & Ford 1996; Chatterjee et al. 2008; Nagasawa et al. 2008; Naoz et al. 2011; Teyssandier et al. 2013; Denham et al. 2019) Furthermore, the fraction of stellar binaries in the field is high ($\sim$40%–70% for $\gtrsim$1 $M_{\odot}$ stars, e.g., Raghavan et al. 2010). The stellar companions may also cause planets to plunge into their host stars (e.g., Lithwick & Naoz 2011; Naoz et al. 2012, 2013a; Veras & Tout 2012; Veras et al. 2013, 2017a, 2017b; Naoz 2016; Veras 2016; Stephan et al. 2017, 2018; Martinez et al. 2019; Veras & Wolszczan 2019).

The interplay between dynamical effects and post-MS evolution can be very rich. An evolving and expanding star may not only engulf planets on initially close-in orbits, but also faraway planets that have had their eccentricities excited due to perturbations from a third companion. Furthermore, an expanding star will experience stronger tidal forces (that scale with its radius) and may shrink a faraway planet's orbit enough to consume it. In either case, the vicinity to the star will heat the planets significantly prior to contact, turning them into "temporary hot Jupiters" (Stephan et al. 2018). However, the mass loss an evolving star undergoes can also expand the orbits, preventing consumption (Valsecchi et al. 2014). This orbital expansion can change the dynamical stability of a system, especially in the presence of companions, which can lead to star–planet collisions at later times (e.g., Hamers & Portegies Zwart 2016; Petrovich & Muñoz 2017; Stephan et al. 2017). The interplay of stellar evolution with dynamical processes can therefore explain a variety of interesting observations (e.g., Xu et al. 2017; Huber et al. 2019; Wang et al. 2019).

Here, we explore the physical processes that a star undergoes as it consumes a planet, for a range of stellar masses and evolutionary phases. The consumption of a planet by a star was considered in the literature as a way to explain a variety of astrophysical phenomena. For example, a planet grazing a stellar surface has been suggested as the cause for the peculiar gas ejections observed from the red giant star V Hydrae (Sahai et al. 2016; Salas et al. 2019). Furthermore, as a planet enters a star's atmosphere, its interaction with the stellar gas has been suggested to result in transit phenomena such as strong stellar wind, as well as strong optical, UV, and X-ray radiation (e.g., Herbig 1977; Retter & Marom 2003; Metzger et al. 2012). Consumption of planets or protoplanetary disk material has also been considered to explain the FU Orionis phenomenon, where a pre-main-sequence star undergoes a relatively fast increase in brightness followed by a gradual decline (e.g., Herbig 1977; Larson 1980; Elbakyan et al. 2019). Moreover,

planet engulfment, similar to binary star interactions, has been considered as a cause for nonspherical planetary nebulae systems (e.g., Morris 1981; Soker 1992, 1994, 1995, 1996, 1998a, 2001; Mastrodemos & Morris 1998; Soker & Harpaz 2000; Livio & Soker 2002; Morris et al. 2006; Kim et al. 2017; Sabach & Soker 2018).

When a star consumes a planet, it may have significant effects on the physical properties of the star. For example, it has been shown that the consumption of a Hot Jupiter by a young star can explain some observed patterns of spin–orbit misalignments in planetary systems (Matsakos & Königl 2015). Recently, a proof-of-concept calculation for main-sequence G- and K-type stars by Qureshi et al. (2018) showed that a consumption of a planet can significantly spin-up a star (lowering the spin period). Furthermore, they showed that this spin period change is consistent with the observed bifurcation of spin periods in young open clusters.

In this work, we integrate all the aforementioned aspects of planet consumption by stars for a comprehensive range of stellar masses and evolutionary phases. We calculate a range of observational signatures that can be used to infer active planetary consumption events (Section 2). In particular, we determine the phase space of planetary and stellar mass and radius that allow the ejection of stellar gas due to grazing interactions (Section 2.1); we calculate the duration and intensity of high-energy UV radiation emitted over the planet's migration through the stellar atmosphere (Section 2.2); and we estimate the new spin periods of post-consumption stars due to angular momentum conservation (Section 2.3).

2. Observable Signatures of Planet Consumption

The consumption of planets by stars involves a multitude of processes and effects as a consequence of angular momentum and energy conservation. As a planet begins to graze and contact the stellar surface, gravitational and tidal interactions can disturb or even eject stellar surface material (e.g., Dosopoulou et al. 2017; Salas et al. 2019). When the planet eventually migrates deeper into the stellar envelope, drag interactions will heat the stellar gas, producing additional luminosity (e.g., Retter & Marom 2003; Bear et al. 2011; Metzger et al. 2012), and transfer angular momentum from the planet's orbit onto the star, changing the stellar spin rate and orientation (e.g., Qureshi et al. 2018). Eventually, the planet will be disrupted and its material will be added to the star, changing its chemical composition. In this section, we investigate all of these consumption signatures and determine their strengths and relevance for different stellar types and evolutionary phases.

2.1. Surface Grazing Interactions

As a planet grazes the surface of a star, it can be expected that stellar surface material will be gravitationally disturbed by the planet, assuming that the planet did not get tidally disrupted beforehand. A planet with radius R_p can approach its host star as close as

$$R_{\rm Roche} \sim kR_p\left(\frac{M_*}{M_p}\right)^{1/3} \sim kR_\odot\left(\frac{R_p}{R_{\rm Jup}}\right)\left(\frac{M_*}{M_\odot}\right)^{1/3}\left(\frac{M_p}{M_{\rm Jup}}\right)^{-1/3} \quad (1)$$

without being disrupted, where M_* and M_p are the star's and planet's masses, respectively, and k is a numerical factor on the order of 1.6–2.4. In general, for any star of solar or heavier mass that has at least slightly evolved toward the later stages or past the main sequence, and which has not yet become a white dwarf or other compact object, this tidal disruption distance is smaller than or on the same order as the radius of the star itself, allowing a planet to reach the stellar surface and to undergo grazing interactions. The star V Hya is very likely an example of this type of interaction.

Over recent decades, the carbon star V Hya has been observed to periodically eject "bullets" of gaseous material (Sahai et al. 2016). These ejections can be explained by the close periastron passage of a substellar companion that grazes the stellar surface, scooping up surface material and ejecting some of it as "bullets" (Salas et al. 2019). A variety of mechanisms have been suggested as the cause of the ejections; however, here we consider a simple ballistic model (e.g., Dosopoulou et al. 2017), where the velocity of the bullets v_b is approximately equal to the sum of the planet's periastron passage velocity and the planet's escape velocity

$$v_b \sim \sqrt{G(M_* + M_p)\frac{1+e_p}{a_p(1-e_p)}} + \sqrt{\frac{2GM_p}{R_p}}, \quad (2)$$

where a_p and e_p are the orbital semimajor axis and eccentricity, respectively.

However, for a bullet to actually leave the star, the bullet velocity must be larger than the stellar escape velocity $v_{\rm esc,*}$ from the periastron, such that

$$v_b \geqslant v_{\rm esc,*}, \quad (3)$$

where v_b is defined in Equation (2) and the escape velocity is simply

$$v_{\rm esc,*} = \sqrt{\frac{2GM_*}{a_p(1-e_p)}}. \quad (4)$$

Equation (3) can yield a specific relation on the mass to radius ratio of planets and stars. Specifically, assuming that the star is much more massive than the planet and that the periastron distance must be approximately the same as the radius of the star, R_*, Equation (3) leads to the condition

$$\frac{M_p}{R_p} \geqslant \frac{M_*}{R_*}\left(\frac{3}{2} + \frac{e_p}{2} - \sqrt{2(1+e_p)}\right), \quad (5)$$

which needs to be fulfilled for ballistic ejections to efficiently leave the stellar system. Note that for extremely eccentric orbits ($e_p \sim 1$), the right side of Equation (5) approaches zero, greatly enhancing ejection likelihood. Figure 1 shows how different types of planets are able to cause V Hya-like ejections, depending on their masses and the stellar evolutionary phases. If a planet does not fulfill Equation (5), its interaction with the stellar surface can only eject stellar material onto bound orbits around the star. This could produce a gas and dust disk or cloud around the star whose mass and extend would depend on the planet's mass.

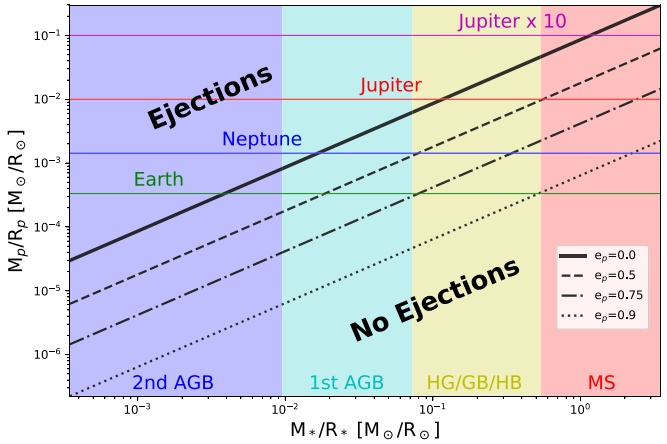

Figure 1. Ejection conditions for a range of planetary masses, stellar types, and orbital eccentricities. The figure plots the ejection conditions outlined in Equation (5), for four different orbital eccentricities e_p: 0 (solid black line), 0.5 (dashed black line), 0.75 (dotted–dashed black line), and 0.95 (dotted black line). Planets whose masses divided by their radius lie above these lines are able to cause V Hya-like ejections for a given star with the corresponding value of its mass divided by its radius. The shaded regions show approximate value ranges of mass divided by radius for different stellar evolutionary phases, for a range of stellar masses. The red region marks values for MS stars, yellow for Hertzsprung gap, giant branch, and helium-burning stars, cyan for first asymptotic giant branch (AGB) stars, and blue for 2nd AGB stars. Note that ejections become easier the more evolved a star is, as its ratio of mass to radius decreases. Values for different example planets are shown as vertical lines: Earth in green, Neptune in blue, Jupiter in red, and a massive Jupiter or small brown dwarf in magenta. While a brown dwarf can cause ejections for any type of star or orbital eccentricity, an Earth-sized planet can only cause them for extremely enlarged AGB stars or at extremely high eccentricities.

2.2. Luminosity and Energy Signatures

After a planet has grazed a stellar surface, it will eventually orbit fully inside the stellar envelope, shedding orbital energy and angular momentum as it spirals further into the star. The planet will interact with the stellar gas through the drag force $f_d = C_d \rho_* {v_k}^2/2$, where C_d is a dimensionless drag coefficient of order unity, ρ_* is the stellar density, and v_k is the relative velocity of the planet within the stellar atmosphere (Metzger et al. 2012). This drag force acts on the planet's effective cross-section A_p, which depends on the size of the stellar scale height $H = k_B T/(\mu \mathrm{m}_H g)$ (here, k_B is the Boltzmann constant, T is the gas temperature, μ is the mean molecular mass of the gas, m_H is the mass of a hydrogen atom, and g is the local gravity), as a difference in distance H inward into the star will increase the density, and thus drag force, by a factor of e. If H is much smaller than the planet's radius R_p, most of the drag will be caused by the part of the planet most inward into the star, and A_p will be of order ${R_p}^{1/2} H^{3/2}$. The drag torque at a given radius r from the stellar center, $f_d A_p \times r$, will thus contribute to the inward migration of the planet with inward radial speed,

$$v_r \sim C_d A_p \frac{\rho_*(r)}{M_p} r v_k(r). \tag{6}$$

The inward radial speed due to drag contributes to the rate of orbital energy dissipation via

$$\dot{E}_\mathrm{orb} = \frac{G M_* M_p v_r}{2r^2}, \tag{7}$$

(Metzger et al. 2012). This energy is added to the stellar gas, heating it up. In general, the travel speed v_k of the planet upon entering the star will be much larger than the stellar atmosphere's sound speed $c_s = \sqrt{\gamma P_*/\rho_*}$; here, γ is the adiabatic index, with a value of 5/3 for ideal gases, and P_* is the gas pressure in the star. The planet will therefore produce a strong shock front as it travels through the stellar atmosphere by which it is orbital energy is dissipated.[4] Assuming the standard Rankine–Hugoniot jump conditions and a strong shock, we can estimate the temperature of the gas behind the shock front as

$$T_\mathrm{shock} = A \frac{\mu \mathrm{m}_H}{k_\mathrm{B}} v_k^2, \tag{8}$$

where A is a numerical factor of order unity depending on the nature of the gas ($\sim$3/16 for an ideal gas). Note that for fully ionized gas in a star $\mu = 0.62$; however, the gas in a red giant is generally not fully ionized preshock, and has a larger value for μ, which has to be taken into account.

The temperature of the shock can be extremely high, potentially reaching several 10,000 K, producing a lot of X-ray and far-UV radiation, as the peak emission strength will occur at $\lambda_\mathrm{max} = b_W/T$, where $b_W \sim 0.28978$ cm K is Wien's displacement constant. The radiation intensity as a function of wavelength for blackbodies with the stellar and shock front temperatures are also shown in Figure 2, following Planck's law. However, the radiation will not necessarily be able to

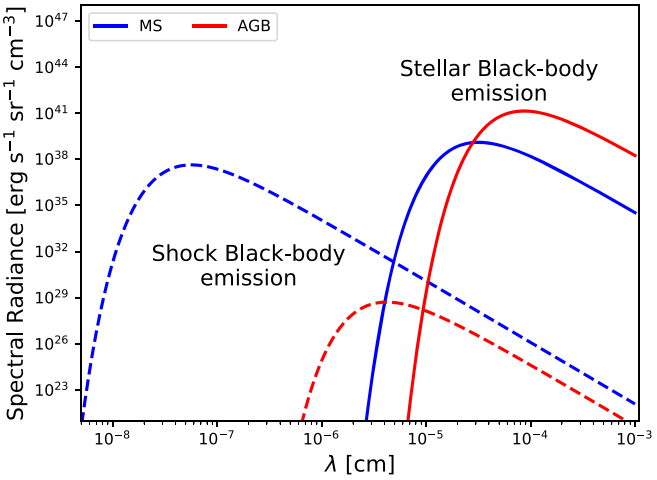

Figure 2. Blackbody Emission of a 2 $M_\odot$ Star vs. (unobscured) shock front blackbody emission during the MS and AGB Phases. The figure shows the blackbody emission spectrum approximating the emission of a 2 $M_\odot$ star (solid lines), compared with the blackbody emission spectrum approximating the possible emission of the hot shock front as a Jupiter-sized planet is consumed by the star (dashed lines). Shown are the spectra during the main sequence (blue lines) and the AGB phases (red lines). Note that as the shock is extremely hot, it emits much stronger in the UV and X-ray than the star itself. However, one would probably not actually see most of this emission; during the main sequence, the power dissipated in the shock can actually surpass the total luminosity of the star, which should drive a wind that eventually obscures the UV emission, turning it into lower temperature thermal emission (Metzger et al. 2012). The energy of the shock would also spread and heat surrounding gases as they mix, reducing the emission temperature. During the AGB phase, as the planet migrates further inward into the stellar envelope, the shock's emission is unlikely to penetrate all the way to the surface of the red giant to be observable. As such, these UV signals would most likely be indicators of extremely recent and ongoing consumption events. For example, for a MS star the energy dissipated in the shock should begin to drive a wind and be obscured about 20 yr into the merger.

[4] Note that there is also a contribution to the inward migration speed and energy dissipation due to tidal forces. This energy is added to the bulk of the star, not the shock front.

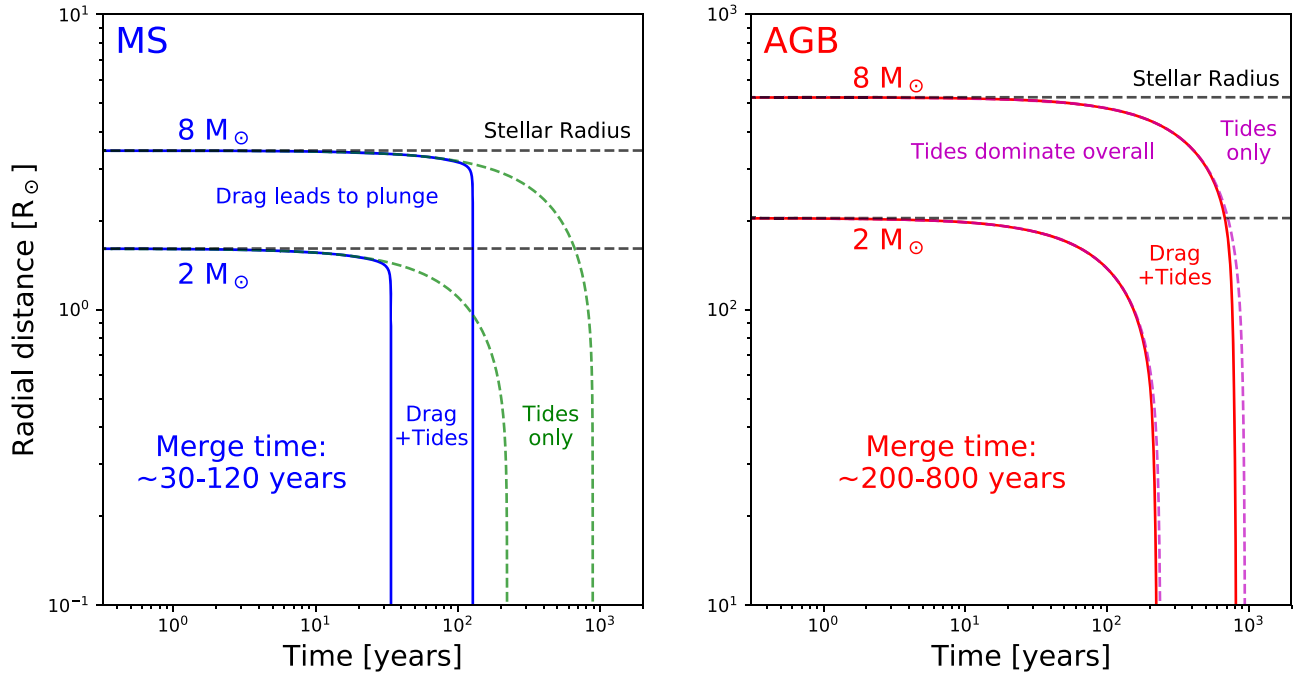

Figure 3. Merging of a Jupiter with a 2 (8) $M_\odot$ Star. This figure shows the inward radial position over time of a Jupiter-sized planet entering either a MS star (left panel) or an AGB star (right panel). Shown are both the migration due to tides alone (dashed green and magenta lines) and due to drag and tides combined (solid blue and red lines), as well as the radius of the star (dashed black lines). Overall, the planet will have fully merged with the MS star after about 30–120 yr, and after about 200–800 yr with the AGB star. The exact time, in all cases, depends strongly on the viscous timescale t_v assumed for the star, as tidal effects dominate while the planets are in the outer layers of the stellar envelope. Here, we assumed $t_v = 1.5$ yr (Hansen 2010; Fabrycky et al. 2007). Indeed, while for MS stars drag forces overtake tidal forces after the planets have migrated to about 90% of the stellar radius, for AGB stars drag forces only begin to dominate at about 50% of the radius. In either case, once drag forces become dominant, the planets will "plunge" into the stellar core on timescales comparable to the planets' orbital periods.

escape the stellar envelope, depending on the optical thickness or ionization state of the gas. Furthermore, the luminosity added to the star can be so large that the immediate region of the shock exceeds its local Eddington limit, which will lead to a wind that will drive an outflow of material from the stellar envelope. This material, in turn, can efficiently block the high-energy radiation emitted by the shock (Metzger et al. 2012), and can also emit additional infrared radiation as it reradiates intercepted stellar radiation. For different stellar types and phases, the reached temperatures and luminosity emitted by the shock vary, as indicated in Figure 2.

We note here that we ignore the potential feedback on stellar structure due to the large amount of energy transferred into the stellar envelope. This feedback would be most relevant for compact stars absorbing large planets. The luminosity generated by the orbital decay, estimated from Equations (6) and (7), can surpass the stellar luminosity by orders of magnitude for a short time during the final "plunge" of the planet into the star (compare also with Figure 2 in MacLeod et al. 2018). This plunge occurs over timescales of hours to days, as can be seen in Figure 3 (see also Metzger et al. 2012). It can therefore be assumed that the interior structure for main-sequence stars or stars in the Hertzsprung gap (i.e., subgiants) would be majorly impacted by the sudden injection of energy, or that the planet itself disintegrates, making our calculations inaccurate to describe the planet's orbital behavior during this final plunge. For evolved and red giant stars on the AGB, however, the energy dissipated due to orbital decay is always much smaller than the star's luminosity and stellar structure should remain mostly unchanged. Stars on the first giant branch (GB) or in the core helium-burning phase (HeB) represent an intermediate case, where we expect the generated orbital decay power to be of similar order to the stellar luminosity during the final plunge. The structure of these stars might therefore be affected by the injected energy, albeit to a lesser degree than for main-sequence or Hertzsprung gap stars.

2.3. Angular Momentum Transfer and Stellar Spin-up

A planet will transfer angular momentum to its star either through tidal forces, mostly important when the planet is still outside or in the outer regions of the star, or through drag forces, especially important when the planet has reached denser interior layers of the star. The tidal friction timescale of the star can be described by (e.g., Hut 1981; Eggleton et al. 1998; Kiseleva et al. 1998; Naoz 2016)

$$t_{\rm TF} = \frac{t_v}{9}\left(\frac{a_p}{r_*}\right)^8 \frac{m_*(r_*)^2}{(m_*(r_*)+M_p)M_p}\frac{1}{(1+k_l)^2}, \quad (9)$$

with t_v and k_l being the stellar viscous timescale and Love number, respectively, a_p being the planet's semimajor axis, M_p being the planetary mass, and m_* being the star's mass interior to the radius r_*. Note that r_* is equal to R_*, the star's outer radius, if the planet has not entered the stellar envelope yet, and is equal to a_p otherwise. This approximation ignores the tidal effects of the stellar material outside of the planet's orbit, as it should generally be insignificant compared to the effects of the stellar interior. The timescale associated with the gas drag forces outlined in Section 2.2 can be described by

$$t_{\rm drag} \sim \frac{R_*}{v_r} \sim {C_d}^{-1}\frac{M_p}{\rho_* A_p v_k}\frac{R_*}{a_p}, \quad (10)$$

(Metzger et al. 2012).

We can apply the timescales for drag and tidal migration, using realistic models of stellar structure for internal density profiles, to estimate the time needed for a planet to fully merge with a star of given mass and evolutionary stage. Here, we assume that the stellar envelope is an $n = 3$ polytrope, with an additional compact core in the case of the red giant. While a MS star might only require a few tens of years to fully merge with a planet, a red giant star might need hundreds of years to do the same, as shown in Figure 3.

In general, drag forces overcome tidal friction eventually after a planet enters a star, both for MS and red giant stars, as can be seen in Figure 3. Indeed, the inward migration speed can become even faster than the orbital speed of the planet, leading to a "plunge," with subsequent disruption of the planet and mixing into the stellar core. Overall, however, an engulfed planet spends the vast majority of its time in the outer layers of the star, where tides dominate over drag. This makes the total lifetime of the planet before the "plunge" highly dependent on the assumed tidal parameters. Once the planet reaches the "plunge" distance, it quickly falls into the core. For a MS star the plunge distance is about one-tenth of the stellar radius (from the surface), for a red giant star the plunge distance is at about half the stellar radius, as can be seen in Figure 3.

Regardless of the mechanism that contributes most to angular momentum transfer and the planet's migration in the stellar envelope, the angular momentum of the planet's orbit will change the spin of the star. Here, we calculate the new spin rates after such spin-up events and estimate under which conditions the spin-up would actually lead to stellar breakup or envelope loss.

The orbital angular momentum of a planet orbiting a star with semimajor axis a_p and eccentricity e is

$$J_{\rm orb} = \frac{M_* M_p}{M_* + M_p}\sqrt{G(M_* + M_p)a_p(1 - e^2)}. \quad (11)$$

Assuming that the planet is much less massive than the star, which is reasonable given the mass ratio of Jupiter to the Sun, and that the planet orbit's closest approach distance $a_p(1 - e)$ must be the same as the size of the star's Roche limit $R_{*,\rm Roche}$, this equation can be simplified to

$$J_{\rm orb} \sim m\sqrt{GM_p R_{*,\rm Roche}(1 + e)}, \quad (12)$$

where we note that e can only vary between values of 0 and 1, thus changing the magnitude of the angular momentum at most by a factor of $\sqrt{2}$. The rotational angular momentum of a spinning star is

$$J_* = I_* \Omega_*, \quad (13)$$

where I_* is the stellar moment of inertia and Ω_* its rotation frequency. Here, we ignore potential differential rotation profiles. For simplicity, we assume that a MS star or a red giant's envelope have a polytropic index of about 3, and basically reaches all the way from the stellar surface to the stellar core, giving the numerical factor 0.08 for the angular moment of inertia calculations. From this, we determine that the stellar angular momentum is about

$$J_{*,\rm env} = I_{*,\rm env}\Omega_{*,\rm env} \sim 0.08 M_{*,\rm env} R_*^2 \Omega_{*,\rm env}, \quad (14)$$

with $I_{*,\rm env}$, $\Omega_{*,\rm env}$, $M_{*,\rm env}$ being the stellar envelope's moment of inertia, rotation rate, and mass, respectively.

When the star's expanding envelope's Roche limit grows past the planet's orbit, the planet will impart its angular momentum onto the star as it eventually spirals inward. The angular momenta must add up such that the envelope's new angular momentum is

$$\begin{aligned} \boldsymbol{J}_{*,\rm env,new} &= \boldsymbol{J}_{*,\rm env} + \boldsymbol{J}_{\rm orb} \\ &= 0.08 M_{*,\rm env} {R_*}^2 \boldsymbol{\Omega}_{*,\rm env,new} \\ &= \Omega_{*,\rm env} + M_p\sqrt{GM_* R_{*,\rm Roche}(1 + e)}\,\hat{\boldsymbol{h}}, \end{aligned} \quad (15)$$

assuming here that the stellar radius does not change due to consumption, no differential rotation, and that the planet's mass, as well as the angular momentum of the planetary spin, are negligible. Note also that the stellar Roche limit can be expressed as

$$R_{*,\rm Roche} = qR_*\left(\frac{M_* + M_p}{M_*}\right)^{1/3} \sim qR_*, \quad (16)$$

with q being a numerical factor assumed here to be about 2.7. The new spin rate $\Omega_{*,\rm env,new}$ is the observable factor, which now becomes

$$\boldsymbol{\Omega}_{*,\rm env,new} = \boldsymbol{\Omega}_{*,\rm env} + 12.5 \times M_p\sqrt{\frac{qGM_*(1 + e)}{M_{*,\rm env}^2 R_*^3}}\,\hat{\boldsymbol{h}}. \quad (17)$$

Using Equation (17), we can now calculate the changes on a red giant star's spin in a variety of scenarios. We use the stellar evolution code SSE (Hurley et al. 2000) to evolve stars of masses between 1 and 8 $M_\odot$ from the beginning of the MS to their widest possible stellar radius during the AGB phase. SSE gives information about the stars' radii, masses, core masses, temperatures, and spin rates during all evolutionary phases. SSE provides fitting formulae based on the stellar evolution models produced by Pols et al. (1998), giving evolution tracks for a wide range of stellar masses and metallicities. In these models, stellar spins are calculated considering the potential division of a star into core and envelope, which is also taken into account in Equation (17), while also considering effects such as magnetic braking for the spin evolution. We adjusted SSE's magnetic braking coefficients by using values from Dobbs-Dixon et al. (2004) for Sun-like stars. We calculate the changes in stellar spin rates and periods upon consumption of planets with varying masses, orbital eccentricities, and spin–orbit angles. The full ranges of tested parameters are shown in Table 1. We compare the changes in spin periods due to consumption during different stellar evolutionary phases, including the MS, GB, the HeB, and the first and second AGB phases. We note here that generally the stellar radius of a star during the HeB phase is smaller than during the GB phase; however, giant planets can still plunge into their host stars during that phase due to effects such as the Eccentric Kozai–Lidov mechanism, in which a companion star can induce high orbital eccentricity on a planet due to gravitational perturbations (e.g., Naoz et al. 2011, 2012, 2013b; Naoz 2016; Stephan et al. 2018). In Figure 4 we show the effects of stellar consumption of prograde-orbiting gas giant planets by stars of different masses and evolutionary phases on the stars' spin periods. In Figures 5 and 6 we show the same for more evolutionary phases and for retrograde planet orbits.

We note here that we calculate the new spin periods only for the time immediately following the planets' consumption and do not predict the further evolution of the spins. Magnetic

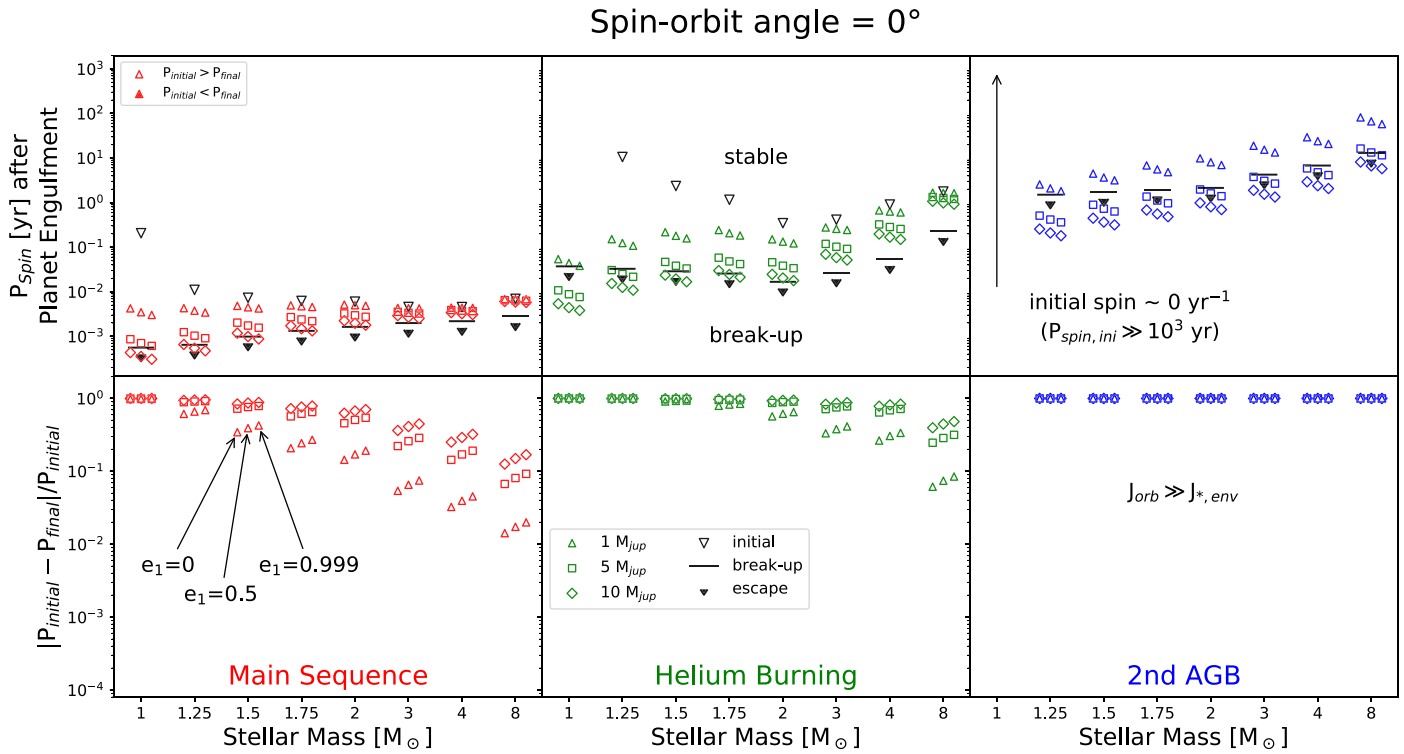

Figure 4. Consumption of prograde-orbiting planets. Shown are the spin periods (upper panels) and fractional changes of the spin periods (lower panels) due to the consumption of prograde-orbiting planets of various masses and various eccentricities for a variety of stellar masses and evolutionary phases. The shown evolutionary phases are main sequence (red), core helium burning (green), and second AGB (blue). The empty black downward triangles show the initial stellar spin periods before consumption, calculated with SSE or based on observations in the case of white dwarfs (Kawaler 2003). The tested planetary masses were 1 $M_{\rm Jup}$ (upward triangles), 5 $M_{\rm Jup}$ (squares), and 10 $M_{\rm Jup}$ (diamonds). For each planetary mass, three orbital eccentricities were tested, shown by groups of three identical symbols; from left to right, the eccentricities were 0, 0.5, and 0.999. The black lines mark the minimum spin periods possible before a star would begin to either lose surface material or be significantly inflated around its equator due to centrifugal forces. The filled-in black downward triangles show spin periods below which surface material would reach escape speeds, being completely lost from the star. These effects are generally more relevant, as shown, for relatively massive planets being consumed by relatively low-mass stars, and for more evolved stars.

Table 1
Parameters

Parameters	Values
M_* [$M_\odot$]	1, 1.25, 1.5, 1.75, 2, 3, 4, 8
M_p [$M_{\rm Jupiter}$]	1, 5, 10
Spin–orbit angle [rad]	0, $\pi/2$, π
e_1	0, 0.5, 0.999

Note. Listed are the relevant parameters for Equation (17) to determine the new stellar spin rate after consumption of a planet.

braking, stellar winds, and further radial inflation or contraction will change the spin periods as the stars continue to evolve. Some previous studies have indicated that the spin-up of red giant stars due to planet consumption could cause important changes to the magnetic fields generated by the stellar envelopes (e.g., Soker 1998b; Privitera et al. 2016b, 2016a), which could strongly impact magnetic braking and mass-loss processes.

2.4. Critical Spin Rates and Stellar Breakup

When calculating the new stellar spins ,we also need to compare it with the rotational breakup speed of the stars, i.e., the rotation rate at which material on the surface of a given star would be launched into orbit, leaving that surface. The simplest definition of this breakup spin period can be written as

$$P_{*,\rm break-up} = 2\pi\sqrt{\frac{{R_*}^3}{GM_*}}. \quad (18)$$

At this spin period, a particle on the stellar surface would remain in circular orbit around the star, ignoring potential additional forces such as radiation pressure or similar effects. If the star spins with a smaller period, material from the stellar surface will be launched into orbit. If the spin period is shorter by a factor of $\sqrt{2}$, material launched from the surface will have escape velocity and leave the star completely. At spin periods between $P_{\rm break-up}$ and $P_{\rm break-up}/\sqrt{2}$, material would be launched onto eccentric orbits, effectively leading to the formation of an extreme equatorial bulge and potentially a gaseous disk around the star. As this takes place the spin periods calculated here would obviously need to be adjusted as the shape of the star changes and potentially loses surface material. We note here that calculated spin speeds beyond the breakup speeds are therefore only an indicator for the formation of oblate stars or circumstellar gaseous disks, not for the actual final observable spins.

As Figures 5 and 6 show, for a wide variety of stellar and planetary masses the addition of the planetary orbital angular momentum would lead to stellar spins exceeding the spin frequencies required for stellar surface material to be ejected, in particular for more evolved stars past GB, but also some

lesser-evolved stars. It therefore seems reasonable to assume that such object might already have been observed by previous surveys. Indicators, for example, would be the presence of infrared-excess radiation from debris disks or ejected stellar gas, together with fast stellar spins. Indeed, some observed systems (e.g., Melis et al. 2009) seem to be good candidates for this process.

2.5. Stellar Chemical Enrichment

The consumption of a planet by a star would also enrich the stellar gas with planetary material. However, at least for gas giants planets, the bulk composition of the planet and the star can be assumed to be very similar, as they are formed from the same protostellar gas and dust disk. Still, there are some cases where the consumption could produce detectable chemical alterations, including lithium enrichment, rocky material enrichment, and white dwarf pollution.

Lithium is easily destroyed in stellar nuclear fusion processes through adding a proton to ^{7}Li, producing two alpha particles. As such, lithium is heavily depleted in fully convective low-mass stars, where material is continuously mixed back into the core fusion zone, and moderately depleted in more massive stars, where lithium is mostly burned during the pre-MS phase but can survive in the stellar atmosphere (e.g., Thévenin et al. 2017). However, many observations have shown that a small number of stars, in particular red giants, show abnormally high lithium abundances, with ideas about the cause including dredge-up, new lithium production, or pollution from interstellar gas, brown dwarfs, or planets (e.g., Alexander 1967; Brown et al. 1989; Montalbán & Rebolo 2002; Aguilera-Gómez et al. 2016; Bharat Kumar et al. 2018; Yan et al. 2018).

Apart from lithium enrichment, it has been suggested that a stellar envelope's metallicity could also be enhanced by absorbing a super-earth or other rocky planetary body (Church et al. 2019). Unfortunately, for a star in isolation, it might be difficult to deduce that the observed metallicity is larger than the primordial metallicity. However, in the case of binary stars, which presumably form with the same primordial metallicities, metal enrichment of one member versus the other might be much easier to determine. Indeed, the binary star pair of HD 240430 and HD 240429 has been suggested to be an example of this scenario, where HD 240430 is estimated to have consumed about 15 $M_\oplus$ of rocky material (Oh et al. 2018).

Elements heavier than hydrogen and helium are expected to sink to the cores of white dwarfs, however about one-quarter to one-third of all white dwarfs still show such heavy elements in their atmospheric spectra (e.g., Zuckerman et al. 2003, 2010; Koester et al. 2014). In general, it is thought that white dwarfs are being polluted by planetary bodies, usually rocky in composition (e.g., Debes & Sigurdsson 2002; Jura 2003; Jura et al. 2009; Zuckerman et al. 2011; Vanderburg et al. 2015; Xu et al. 2016; Veras et al. 2017a, 2017b), though some icy bodies containing volatile compounds have also been shown to contribute (Stephan et al. 2017; Xu et al. 2017). Furthermore, even gas giants could theoretically be brought onto extremely eccentric orbits, getting close enough to the white dwarfs for tidal disruption and eventual pollution (Stephan et al. 2017, 2018). The material brought onto a white dwarf from such a massive pollution source could majorly alter the composition of the white dwarf; many white dwarfs are so called helium white dwarfs, with little to no hydrogen left in their atmosphere. A gas giant planet with a mass in the range or 1 to 10 $M_{\rm Jup}$, roughly 0.001–0.01 $M_\odot$, could cover the white dwarf with a hydrogen atmosphere. Some of the material could also produce second-generation planets or planetary nebulae (e.g., Bear & Soker 2015; van Lieshout et al. 2018).

3. Discussion

We have studied the variety of consequences due to planetary consumption throughout a star's lifetime. Planetary consumption is expected to be a common outcome of dynamically hot systems (e.g., Rasio & Ford 1996; Chatterjee et al. 2008; Nagasawa et al. 2008; Veras & Ford 2010; Naoz et al. 2012; Valsecchi et al. 2014; Petrovich 2015; Petrovich & Muñoz 2017; Stephan et al. 2017, 2018; Denham et al. 2019).

Considering a wide range of stellar masses (1–8 $M_\odot$) and a wide range of planetary masses (1 $M_\oplus$–10 $M_{\rm J}$), we examined the effects of planet consumption on a host star. We note here that these calculations are agnostic to the process leading to Roche-limit crossing. The initial stage of star–planet interaction, where the planet interacts with the surface of the star, can have large observable effects. It may lead to ejections of material, either resulting in winds and planetary nebulae (e.g., Livio & Soker 2002), or even violent, periodic ejections (as was shown for the case of V Hydrae ejections Salas et al. 2019). The ejection of stellar material due to grazing interactions depends on the star's and planet's mass and size, as well as the orbital eccentricity. We quantified the phase space, considering ballistics ejections,[5] at which ejection of material is expected at any given point of a star's lifetime (see Figure 1). In particular, we find that Jupiter mass planets (or higher masses) are efficient in ejecting material over most of the stellar lifetime and for most stellar masses, even for circular orbits. Smaller planets on eccentric orbits can also lead to material ejection rather efficiently. Because the escape velocity from the surface of a star on its second AGB phase is relatively low (a few tens of km s^{-1}), even small, Earth-like planets are sufficient to cause ejections, albeit small ones.

As a planet migrates further into a star's atmosphere, it begins to experience gas drag and creates a hot shock as it loses orbital energy. This shock can produce observable UV radiation. For MS stars (blue lines in Figure 2) the shock's blackbody emission intensity can be comparable to the star's radiation (as was shown previously in Metzger et al. 2012). However, the large amount of energy released can drive a wind, obstructing direct observation of the UV emission and converting it into cooler thermal radiation. During the AGB phase the planet's shock radiation is much less intense than the stellar emission. Thus, while it has less power, it may add a small far-UV component to a predominantly visual emission (see red lines in Figure 2). We estimated the timescales over which the consumption takes place and over which the additional UV signals might be observable. The migration of a planet just inside the surface of a star will mostly be dominated by tides (as shown in Figure 3) until drag becomes dominant and "plunges" the planet into the stellar core. To reach this phase, it takes on the order of a few decades for MS stars and on the order of a few centuries for red giant stars, over which UV signals and shock effects should be visible.

[5] Note that there are variety of processes that may lead to ejections (e.g., Goodson & Winglee 1999; Fendt 2003). Here we adopted the simplest one, which makes no assumptions on magnetic fields or accretion disks.

Once the planet is finally consumed by the star, we estimated the resulting stellar spin periods from angular momentum conservation.[6] We found that MS stars, post-consumption, should be rapidly spinning (consistent with Qureshi et al. 2018) and that the consumption can significantly alter the star's axis of rotation (consistent with Matsakos & Königl 2015). Red giant stars, post-consumption, can often reach spin speeds at or beyond breakup speeds, indicating that these stars would undergo mass loss from their surface or are strongly tidally distorted into a flattened shape or will become enshrouded by ejected gas. This can also apply to smaller mass stars consuming massive planets or brown dwarfs. Finally, we also showed that white dwarfs can also be significantly spun up, if the angular momentum of a planet can be efficiently transferred to the star. This feature may explain some observed white dwarfs with very short spin periods, such as SDSS J0837 +1856 (e.g., Hermes et al. 2017a, 2017b).

Already, observations of short-period planets show that some may have decaying orbits that will eventually let them be consumed by their host star. For example, WASP-12b is a Jupiter size planet that is on a decaying orbit around a 1.35 $M_{\odot}$ star (e.g., Li et al. 2010; Patra et al. 2017). Based on our calculations (e.g., Figures 4 and 6), we predict that the spin period of WASP-12, upon consumption of this planet, may decrease by a factor of two (prograde orbit), or would be completely flipped (retrograde orbit). Additional planets that are estimated to be on decaying orbits have also been observed (e.g., Gaudi et al. 2017; Johnson et al. 2018; Johns et al. 2019; Labadie-Bartz et al. 2019; Rodriguez et al. 2019).

While the observation of an active consumption event might be challenging for a MS star, given the short timescale of a few decades per consumption event, for a red giant star the timescales are relatively favorable, as consumption events would last for centuries or even millennia. Given lifetimes of a few hundred thousand to a few million years for the AGB phase, the chance to observe an engulfment (assuming that every AGB star engulfs a planet) would be on the order of a few tenths to about 1%. Beyond direct observations, the pre- and post-consumption signatures described in this work may provide several avenues to indirectly infer the existence of a planet around a given star. Future *Hubble Space Telescope* (*HST*) and *James Webb Space Telescope* (*JWST*) observations may detect some of the signatures described here (similar to the gas ejections from V Hydrae described by Sahai et al. 2016).

We thank the anonymous referee for their comments and suggestions to improve this paper. A.P.S. and S.N. acknowledge partial support from the NSF through grant No. AST-1739160. S.N. thanks Howard and Astrid Preston for their generous support. We thank Noam Soker and Brian Metzger for helpful comments and discussions.

Appendix
Post-planet-consumption Spin Periods

Here, we provide expanded versions of Figure 4, showing the stellar pre- and post-consumption spin periods for stars during the main sequence, first giant branch, helium burning, first asymptotic giant branch, second asymptotic giant branch, and as white dwarfs. The values are calculated for a range of stellar and planetary masses, and varying orbital eccentricities. Figure 5 shows the values assuming a prograde orbit of the planet during engulfment, Figure 6 assumes a retrograde orbit. We also show the fractional change in spin periods due to engulfment, and mark spin periods that would surpass breakup speed, highlighting engulfment events that would most likely lead to stellar mass loss through gas ejections or decretion disks.

[6] Note that angular momentum may not be strictly conserved due to mass losses and winds. The consequences of these processes are beyond the scope of this paper.

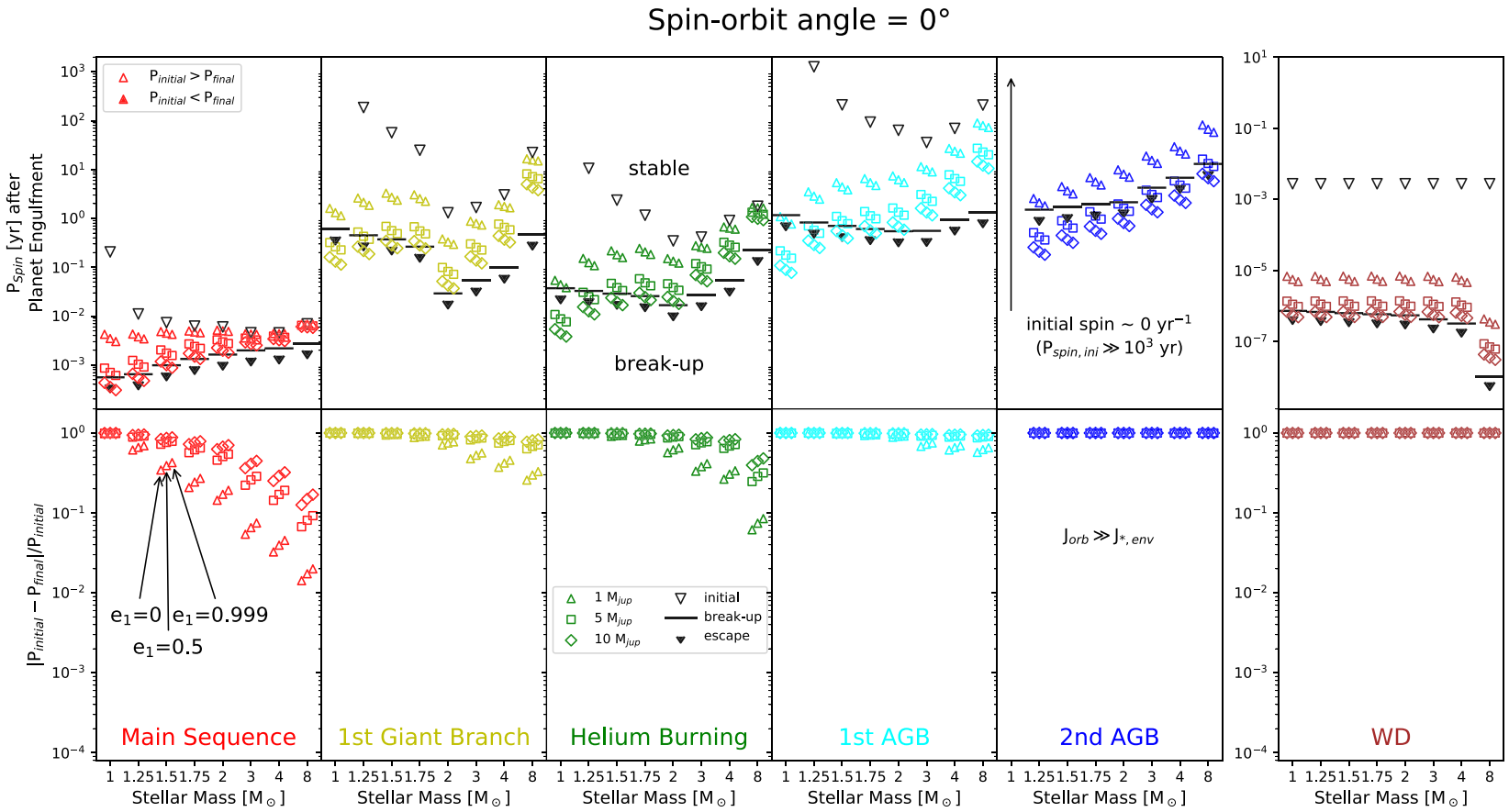

Figure 5. Consumption of prograde-orbiting Planets (extended). This figure is similar to Figure 4, however it also includes the results for a larger number of stellar evolution phases. The shown evolutionary phases are main sequence (red), first giant branch (yellow), core helium burning (green), first AGB (cyan), second AGB (blue), and white dwarfs (brown). The empty black downward triangles show the initial stellar spin periods before consumption, calculated with SSE or based on observations in the case of white dwarfs (Kawaler 2003). The tested planetary masses were 1 M_{Jup} (upward triangles), 5 M_{Jup} (squares), and 10 M_{Jup} (diamonds). For each planetary mass, three orbital eccentricities were tested, shown by groups of three identical symbols; from left to right, the eccentricities were 0, 0.5, and 0.999. The black lines mark the minimum spin periods possible before a star would begin to either lose surface material or be significantly inflated around its equator due to centrifugal forces. The filled-in black downward triangles show spin periods below which surface material would reach escape speeds, being completely lost from the star. These effects are generally more relevant, as shown, for relatively massive planets being consumed by relatively low-mass stars, and for more evolved stars.

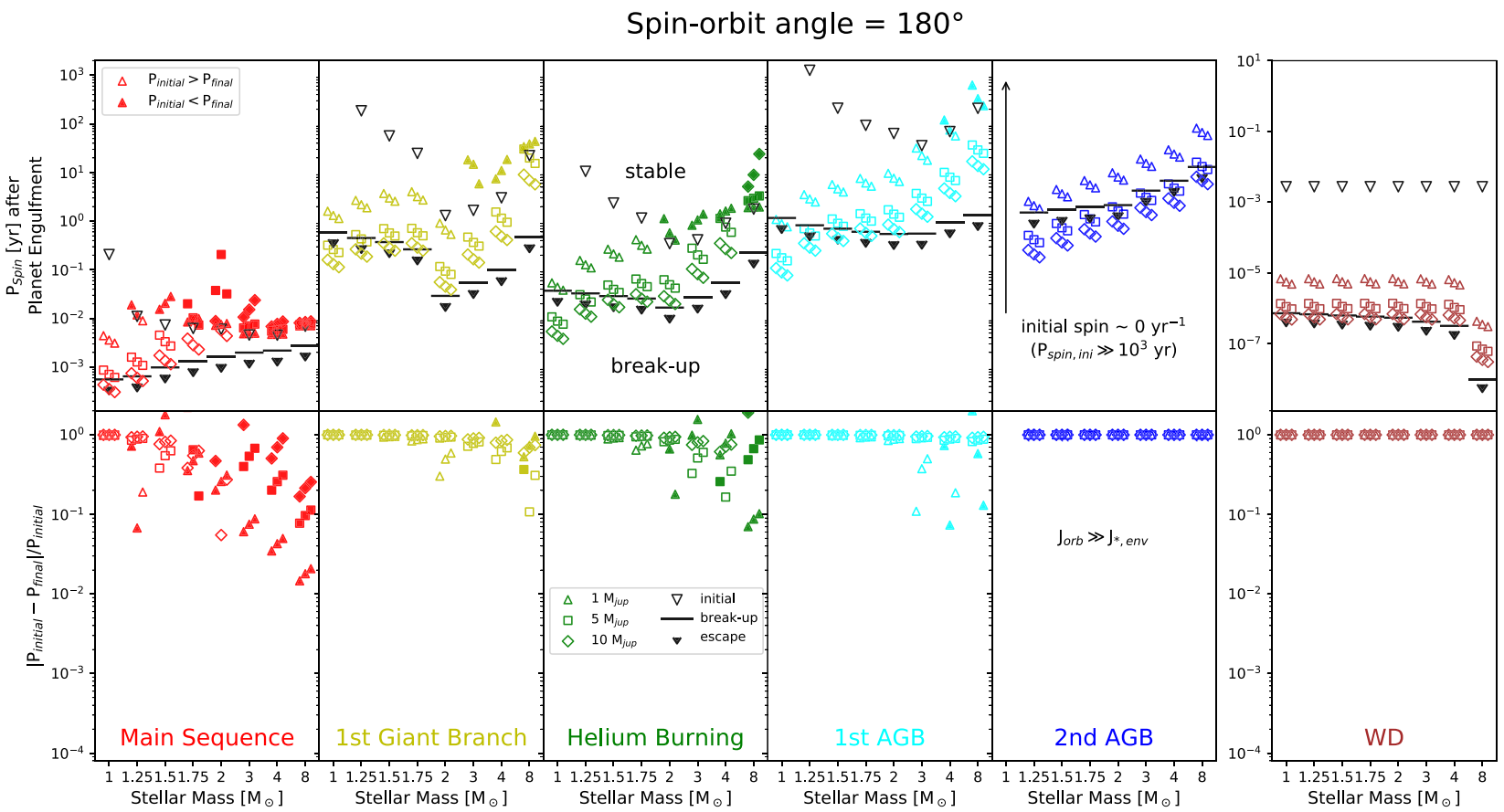

Figure 6. Consumption of retrograde-orbiting planets. This figure is similar to Figure 5, however here the planets orbited the stars in retrograde orbits relative to the preconsumption stellar spin orientation. As a result, it is possible to not just increase a star's spin velocity due to the planets' consumption, but also to instead slow them down. This is shown by the filled-in symbols in the upper and lower panels and appears to be most relevant for massive pre-AGB stars. In all other cases, the angular momentum added by the planets overcomes the stars' own angular momentum, resulting in still faster rotation; however, in that case, the spin direction is reversed relative to the initial spin.

ORCID iDs

Alexander P. Stephan https://orcid.org/0000-0001-8220-0548
Smadar Naoz https://orcid.org/0000-0002-9802-9279
B. Scott Gaudi https://orcid.org/0000-0003-0395-9869

References

Aguilera-Gómez, C., Chanamé, J., Pinsonneault, M. H., & Carlberg, J. K. 2016, ApJ, 829, 127
Alexander, J. B. 1967, Obs, 87, 238
Barnes, J. W., van Eyken, J. C., Jackson, B. K., Ciardi, D. R., & Fortney, J. J. 2013, ApJ, 774, 53
Bear, E., Kashi, A., & Soker, N. 2011, MNRAS, 416, 1965
Bear, E., & Soker, N. 2015, MNRAS, 450, 4233
Bharat Kumar, Y., Singh, R., Eswar Reddy, B., & Zhao, G. 2018, ApJL, 858, L22
Brown, J. A., Sneden, C., Lambert, D. L., & Dutchover, E. J. 1989, ApJS, 71, 293
Charpinet, S., Fontaine, G., Brassard, P., et al. 2011, Natur, 480, 496
Chatterjee, S., Ford, E. B., Matsumura, S., & Rasio, F. A. 2008, ApJ, 686, 580
Church, R. P., Mustill, A. J., & Liu, F. 2019, MNRAS, 491, 2391
Debes, J. H., & Sigurdsson, S. 2002, ApJ, 572, 556
Denham, P., Naoz, S., Hoang, B.-M., Stephan, A. P., & Farr, W. M. 2019, MNRAS, 482, 4146
Dobbs-Dixon, I., Lin, D. N. C., & Mardling, R. A. 2004, ApJ, 610, 464
Dosopoulou, F., Naoz, S., & Kalogera, V. 2017, ApJ, 844, 12
Eggleton, P. P., Kiseleva, L. G., & Hut, P. 1998, ApJ, 499, 853
Elbakyan, V. G., Vorobyov, E. I., Rab, C., et al. 2019, MNRAS, 484, 146
Fabrycky, D. C., Johnson, E. T., & Goodman, J. 2007, ApJ, 665, 754
Fendt, C. 2003, A&A, 411, 623
Gaudi, B. S., Stassun, K. G., Collins, K. A., et al. 2017, Natur, 546, 514
Gettel, S., Wolszczan, A., Niedzielski, A., et al. 2012, ApJ, 745, 28
Goodson, A. P., & Winglee, R. M. 1999, ApJ, 524, 159
Hamers, A. S., & Portegies Zwart, S. F. 2016, MNRAS, 462, L84
Hansen, B. M. S. 2010, ApJ, 723, 285
Herbig, G. H. 1977, ApJ, 217, 693
Hermes, J. J., Gänsicke, B. T., Kawaler, S. D., et al. 2017b, ApJS, 232, 23
Hermes, J. J., Kawaler, S. D., Romero, A. D., et al. 2017a, ApJL, 841, L2
Howard, A. W., Marcy, G. W., Bryson, S. T., et al. 2012, ApJS, 201, 15
Huber, D., Chaplin, W. J., Chontos, A., et al. 2019, AJ, 157, 245
Hurley, J. R., Pols, O. R., & Tout, C. A. 2000, MNRAS, 315, 543
Hut, P. 1981, A&A, 99, 126
Johns, D., Reed, P. A., Rodriguez, J. E., et al. 2019, AJ, 158, 78
Johnson, J. A., Apps, K., Gazak, J. Z., et al. 2011, ApJ, 730, 79
Johnson, M. C., Rodriguez, J. E., Zhou, G., et al. 2018, AJ, 155, 100
Jura, M. 2003, ApJL, 584, L91
Jura, M., Muno, M. P., Farihi, J., & Zuckerman, B. 2009, ApJ, 699, 1473
Kawaler, S. D. 2003, arXiv:astro-ph/0301539
Kim, H., Trejo, A., Liu, S.-Y., et al. 2017, NatAs, 1, 0060
Kiseleva, L. G., Eggleton, P. P., & Mikkola, S. 1998, MNRAS, 300, 292
Klein, B., Jura, M., Koester, D., & Zuckerman, B. 2011, ApJ, 741, 64
Klein, B., Jura, M., Koester, D., Zuckerman, B., & Melis, C. 2010, ApJ, 709, 950
Koester, D., Gänsicke, B. T., & Farihi, J. 2014, A&A, 566, A34
Labadie-Bartz, J., Rodriguez, J. E., Stassun, K. G., et al. 2019, ApJS, 240, 13
Larson, R. B. 1980, MNRAS, 190, 321
Li, S.-L., Miller, N., Lin, D. N. C., & Fortney, J. J. 2010, Natur, 463, 1054
Lithwick, Y., & Naoz, S. 2011, ApJ, 742, 94
Livio, M., & Soker, N. 2002, ApJL, 571, L161
MacLeod, M., Cantiello, M., & Soares-Furtado, M. 2018, ApJL, 853, L1
Martinez, M., Stone, N. C., & Metzger, B. D. 2019, MNRAS, 489, 5119
Mastrodemos, N., & Morris, M. 1998, ApJ, 497, 303
Matsakos, T., & Königl, A. 2015, ApJL, 809, L20
Melis, C., Farihi, J., Dufour, P., et al. 2011, ApJ, 732, 90
Melis, C., Zuckerman, B., Song, I., Rhee, J. H., & Metchev, S. 2009, ApJ, 696, 1964
Metzger, B. D., Giannios, D., & Spiegel, D. S. 2012, MNRAS, 425, 2778
Montalbán, J., & Rebolo, R. 2002, A&A, 386, 1039
Morris, M. 1981, ApJ, 249, 572
Morris, M., Sahai, R., Matthews, K., et al. 2006, in IAU Symp. 234, Planetary Nebulae in our Galaxy and Beyond, ed. M. J. Barlow & R. H. Méndez (Cambridge: Cambridge Univ. Press), 469
Nagasawa, M., Ida, S., & Bessho, T. 2008, ApJ, 678, 498
Naoz, S. 2016, ARA&A, 54, 441
Naoz, S., Farr, W. M., Lithwick, Y., Rasio, F. A., & Teyssandier, J. 2011, Natur, 473, 187
Naoz, S., Farr, W. M., Lithwick, Y., Rasio, F. A., & Teyssandier, J. 2013a, MNRAS, 431, 2155
Naoz, S., Farr, W. M., & Rasio, F. A. 2012, ApJL, 754, L36
Naoz, S., Kocsis, B., Loeb, A., & Yunes, N. 2013b, ApJ, 773, 187
Niedzielski, A., Villaver, E., Nowak, G., et al. 2016, A&A, 588, A62
Niedzielski, A., Wolszczan, A., Nowak, G., et al. 2015, ApJ, 803, 1
Nowak, G., Niedzielski, A., Wolszczan, A., Adamów, M., & Maciejewski, G. 2013, ApJ, 770, 53
Oh, S., Price-Whelan, A. M., Brewer, J. M., et al. 2018, ApJ, 854, 138
Patra, K. C., Winn, J. N., Holman, M. J., et al. 2017, AJ, 154, 4
Petrovich, C. 2015, ApJ, 799, 27
Petrovich, C., & Muñoz, D. J. 2017, ApJ, 834, 116
Pols, O. R., Schröder, K.-P., Hurley, J. R., Tout, C. A., & Eggleton, P. P. 1998, MNRAS, 298, 525
Privitera, G., Meynet, G., Eggenberger, P., et al. 2016a, A&A, 593, A128
Privitera, G., Meynet, G., Eggenberger, P., et al. 2016b, A&A, 593, L15
Qureshi, A., Naoz, S., & Shkolnik, E. L. 2018, ApJ, 864, 65
Raghavan, D., McAlister, H. A., Henry, T. J., et al. 2010, ApJS, 190, 1
Rasio, F. A., & Ford, E. B. 1996, Sci, 274, 954
Reffert, S., Bergmann, C., Quirrenbach, A., Trifonov, T., & Künstler, A. 2015, A&A, 574, A116
Retter, A., & Marom, A. 2003, MNRAS, 345, L25
Rodriguez, J. E., Quinn, S. N., Huang, C. X., et al. 2019, AJ, 157, 191
Sabach, E., & Soker, N. 2018, MNRAS, 473, 286
Sahai, R., Scibelli, S., & Morris, M. R. 2016, ApJ, 827, 92
Salas, J. M., Naoz, S., Morris, M. R., & Stephan, A. P. 2019, MNRAS, 487, 3029
Soker, N. 1992, ApJ, 386, 190
Soker, N. 1994, PASP, 106, 59
Soker, N. 1995, MNRAS, 274, 147
Soker, N. 1996, ApJL, 460, L53
Soker, N. 1998a, AJ, 116, 1308
Soker, N. 1998b, MNRAS, 299, 1242
Soker, N. 2001, MNRAS, 324, 699
Soker, N., & Harpaz, A. 2000, MNRAS, 317, 861
Stephan, A. P., Naoz, S., & Gaudi, B. S. 2018, AJ, 156, 128
Stephan, A. P., Naoz, S., & Zuckerman, B. 2017, ApJL, 844, L16
Teyssandier, J., Naoz, S., Lizarraga, I., & Rasio, F. A. 2013, ApJ, 779, 166
Thévenin, F., Oreshina, A. V., Baturin, V. A., et al. 2017, A&A, 598, A64
Valsecchi, F., Rasio, F. A., & Steffen, J. H. 2014, ApJL, 793, L3
Vanderburg, A., Johnson, J. A., Rappaport, S., et al. 2015, Natur, 526, 546
van Lieshout, R., Kral, Q., Charnoz, S., Wyatt, M. C., & Shannon, A. 2018, MNRAS, 480, 2784
Veras, D. 2016, RSOS, 3, 150571
Veras, D., Carter, P. J., Leinhardt, Z. M., & Gänsicke, B. T. 2017a, MNRAS, 465, 1008
Veras, D., & Ford, E. B. 2010, ApJ, 715, 803
Veras, D., Georgakarakos, N., Dobbs-Dixon, I., & Gänsicke, B. T. 2017b, MNRAS, 465, 2053
Veras, D., Mustill, A. J., Bonsor, A., & Wyatt, M. C. 2013, MNRAS, 431, 1686
Veras, D., & Tout, C. A. 2012, MNRAS, 422, 1648
Veras, D., & Wolszczan, A. 2019, MNRAS, 488, 153
Wang, S., Jones, M., Shporer, A., et al. 2019, AJ, 157, 51
Xu, S., Jura, M., Dufour, P., & Zuckerman, B. 2016, ApJL, 816, L22
Xu, S., Zuckerman, B., Dufour, P., et al. 2017, ApJL, 836, L7
Yan, H.-L., Shi, J.-R., Zhou, Y.-T., et al. 2018, NatAs, 2, 790
Zuckerman, B., Koester, D., Dufour, P., et al. 2011, ApJ, 739, 101
Zuckerman, B., Koester, D., Reid, I. N., & Hünsch, M. 2003, ApJ, 596, 477
Zuckerman, B., Melis, C., Klein, B., Koester, D., & Jura, M. 2010, ApJ, 722, 725